# Elastic scattering from a potential. Estimating total cross section while applying Numerov's method to the radial part of the time-independent Schrödinger equation.

Reinaldo Magallanes Saunders*

October 2020

## 1 Introduction

The main objective of this assignment is to calculate the total cross section for a simple scattering problem. The core of the assignment is the approximation of solutions to the radial part of the time-independent Schrödinger equation and the calculation of the phase shifts. This will be done using a script in Python that implements Numerov's algorithm, tailored for this particular problem.

## 2 Statement of the Problem

For the case of elastic scattering between two spinless, non-relativistic particles, it can be shown[1], when the interaction between said particles depends only on their relative distance $r$, that this can be reduced to solving the following Schrödinger equation:

$$\left[-\frac{\hbar^2}{2\mu}\nabla^2 + V(r)\right]\Psi(\mathbf{r}) = E\Psi(\mathbf{r}) \tag{1}$$

for a fictitious particle with a reduced mass $\mu$.

We can think of equation (1) as representing the scattering of a particle of mass $\mu$ from a fixed scattering center that is described by $V(r)$, where $r$ is the distance from the particle to the center.

We assume that $V(r)$ has a finite range, therefore the particle behaves as a free particle before collision and can be described by a plane wave. Then, after scattering has taken place, the total wave consists of a superposition of the incident plane wave, propagating in the forward direction, and the scattered wave that propagates along some direction $(\theta, \phi)$. Then:

*e-mail: rei.magallanes@gmail.com

$$\Psi(\mathbf{r}) \sim e^{i\mathbf{k_0}\cdot\mathbf{r}} + \frac{f(\theta,\phi)}{r} e^{i\mathbf{k}\cdot\mathbf{r}} \tag{2}$$

where $\mathbf{k_0}$ is the wave vector associated with the incident particle, $\mathbf{k}$ is the wave vector associated with the scattered particle, $\theta$ is the angle between $\mathbf{k}$ and $\mathbf{k_0}$, and $f(\theta,\phi)$ is the scattering amplitude.

If we assume elastic scattering, for which $|\mathbf{k}| = |\mathbf{k_0}|$, and spherical symmetry, then:

$$\Psi(\mathbf{r}) \sim e^{ikr\cos\theta} + \frac{f(\theta)}{r} e^{ikr} \tag{3}$$

The differential cross section $d\sigma/d\Omega$ is the probability per unit time that a particle crosses the surface element $dS = r^2 d\Omega$, where $\Omega$ is the solid angle. The total cross section is given by

$$\sigma_t = \int \frac{d\sigma}{d\Omega} d\Omega \tag{4}$$

It can be shown[1], that the differential cross section is related to the scattering amplitude in the form

$$\frac{d\sigma}{d\Omega} = |f(\theta)|^2 \tag{5}$$

Now, the general expression for the wave function will be

$$\Psi(\mathbf{r}) = \sum_{l=0}^{\infty} \sum_{m=-l}^{l} A_{lm} \frac{\chi_l(r)}{r} Y_{lm}(\theta,\phi) \tag{6}$$

which, since we assume spherical symmetry, will reduce to

$$\Psi(\mathbf{r}) = \sum_{l=0}^{\infty} A_l \frac{\chi_l(r)}{r} P_l(\cos\theta) \tag{7}$$

Here, the functions $\chi_l(r)$ are the solutions for positive energy with an angular momentum $l$ of the radial Schrödinger equation:

$$\frac{\hbar^2}{2\mu}\frac{d^2\chi_l(r)}{dr^2} + \left[E - V(r) - \frac{\hbar^2 l(l+1)}{2\mu r^2}\right]\chi_l(r) = 0 \quad for \quad E = \frac{\hbar^2 k^2}{2\mu} \tag{8}$$

The asymptotic behaviour at large $r$ of $\chi_l$ is[2]:

$$\chi_l(r) \sim kr[j_l(kr)\cos\delta_l - n_l(kr)\sin\delta_l] \quad for \quad r \to \infty \tag{9}$$

where $j_l$ and $n_l$ are the spherical Bessel functions, which are solutions of the radial equation for $R_l(r)$, $rR_l(r) = \chi_l(r)$, for zero potential.

It can be shown[1], that $\delta_l$ is a real angle which vanishes for all values of $l$ in the absence of the scattering potential. The quantities $\delta_l$ are called phase shifts, and they measure[1], at large values of $r$, the degree to which $R_l(r)$ differs from $j_l(kr)$.

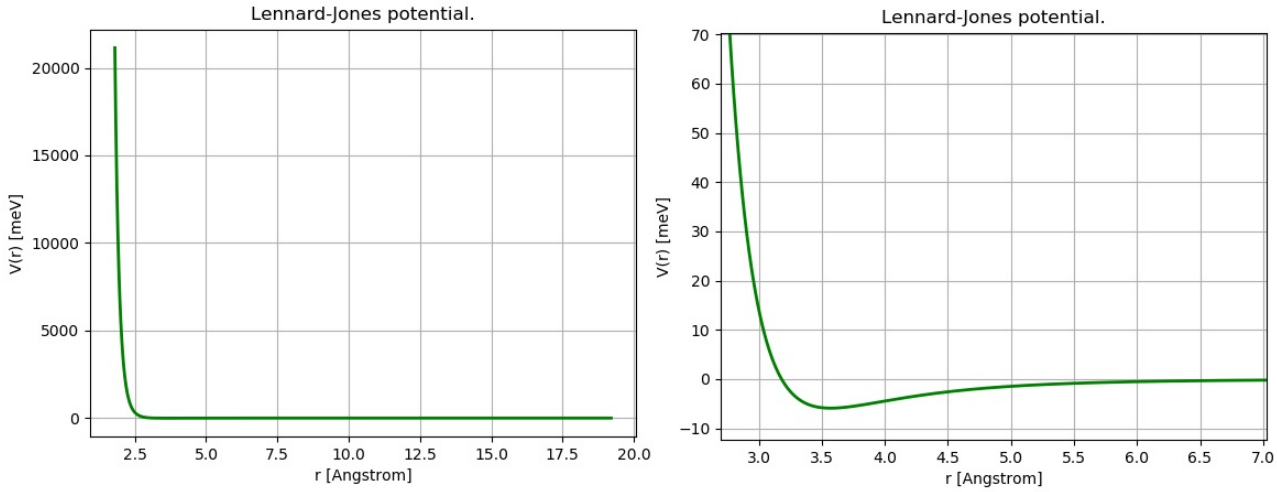


Figure 1: Lennard-Jones potential.

Since they appear in the presence of the scattering potential, it can be expected that the cross section will depend on $\delta_l$. This is, in fact, the case, and it can be shown[1] that

$$f(\theta) = \frac{1}{k}\sum_{l=0}^{\infty}(2l+1)e^{i\delta_l}\sin\delta_l P_l(\cos\theta) \tag{10}$$

and

$$\frac{d\sigma}{d\Omega} = |f(\theta)|^2 = \frac{1}{k^2}\left|\sum_{l=0}^{\infty}(2l+1)e^{i\delta_l}\sin\delta_l P_l(\cos\theta)\right|^2 \tag{11}$$

Therefore, we get:

$$\sigma_t = \sum_{l=0}^{\infty}\sigma_l = \frac{4\pi}{k^2}\sum_{l=0}^{\infty}(2l+1)\sin^2\delta_l \quad , \quad k^2 = \frac{2\mu E}{\hbar^2} \tag{12}$$

where the terms $\sigma_l$ are the partial cross sections corresponding to the scattering of particles in various angular momentum states.

Since the phase shifts $\delta_l$ are functions of the energy, they contain all the information needed to know the scattering properties of a potential.

The potential chosen is the Lennard-Jones potential:

$$V(r) = \epsilon\left[\left(\frac{\varsigma}{r}\right)^{12} - 2\left(\frac{\varsigma}{r}\right)^{6}\right] \quad where \quad \epsilon = 5.9meV, \quad \varsigma = 3.57\text{Å} \tag{13}$$

This potential has a minimum $V_{min} = -\epsilon$ for $r = \varsigma$, is zero for $r = \varsigma/2^{1/6}$ and becomes strongly positive for small values of $r$. It can be seen in Figure 1.

# 3 Algorithm and Implementation

The algorithm will calculate the total cross section and the partial cross sections from equation (12) and it has three main parts.

First, the solution of the radial part of the Schrödinger equation (8) with the scattering potential given by (13). This will be done using Numerov's method with an equispaced grid and integrating forward.

Since the potential has a term that goes as $r^{-12}$, the integration will start from:

$$r_{min} = \frac{\varsigma}{2} \approx 1.8 \tag{14}$$

This was chosen because here the wave function is small but not too close to zero[2].

The first two points for the integration were calculated assuming the following behaviour as $r \to 0$. Combining equations (8) and (13) we get the asymptotic equation:

$$\frac{\hbar^2}{2\mu}\frac{d^2\chi(r)}{dr^2} - \epsilon\frac{\varsigma^{12}}{r^{12}}\chi(r) \sim 0 \quad therefore \quad \frac{d^2\chi(r)}{dr^2} \sim \frac{2\mu\epsilon}{\hbar^2}\frac{\varsigma^{12}}{r^{12}}\chi(r) \tag{15}$$

Then, we can propose[2]:

$$\chi(r) \sim \exp\left(-\sqrt{\frac{2\mu\epsilon\varsigma^{12}}{25\hbar^2}}r^{-5}\right) \quad for \quad r \to 0 \tag{16}$$

This introduces an error of lower order than Numerov's method[2], therefore is not very accurate.

This leads to the choice in units. It will be convenient to choose units in which $\hbar^2/2\mu$ is a number of the order of 1. This is why we choose to express energies in $meV$ and distances in Å. We also take $\mu$ to be the mass of the proton.

Then, the calculation of the phase shifts. This will be done by comparing functions of the form (9) at two different values $r_1$ and $r_2$. This values will be larger than the distance $r_{max}$ where the potential can be ignored. If we take the ratio between this two functions we get:

$$\kappa = \frac{r_1\chi_l(\mathbf{r_2})}{r_2\chi_l(\mathbf{r_1})} = \frac{j_l(kr_2) - n_l(kr_2)\tan\delta_l}{j_l(kr_1) - n_l(kr_1)\tan\delta_l} \tag{17}$$

Therefore:

$$\tan\delta_l = \frac{\kappa j_l(kr_1) - j_l(kr_2)}{\kappa n_l(kr_1) - n_l(kr_2)} \tag{18}$$

Some care is required here. It could be that the denominator in either of these two equations gets close to zero, resulting in *RuntimeWarning* type warnings. This leads to either $\kappa$ or $\tan\delta_l$ being *NaN* type variables and therefore the rest of the loop fails.

It is here that we choose the value $r_{max}$ where the integration will end. We take:

$$r_{max} = 5\varsigma \approx 18 \tag{19}$$

Good choices[2] for $r_1$ and $r_2$ are:

$$r_2 = r_{max} + \frac{\lambda}{4} \quad and \quad r_1 = r_2 - \frac{\lambda}{4} \quad where \quad \lambda = \frac{2\pi}{k} \tag{20}$$

Here $r_1$ is not necessarily equal to $r_{max}$. This will be handled in terms of the step in the radial grid, potentially leading to a different value. These choices are made in order to avoid the warnings mentioned before.

The spherical Bessel functions $j_l$ and $n_l$ will be computed using the following recurrence relation:

$$f_{n-1}(z) + f_{n+1}(z) = \frac{2n+1}{z} f_n(z) \tag{21}$$

which both functions satisfy. To start we will use:

$$\begin{aligned} j_{-1}(z) = \frac{\cos z}{z} \quad , \quad j_0(z) = \frac{\sin z}{z} \\ n_{-1}(z) = \frac{\sin z}{z} \quad , \quad n_0(z) = -\frac{\cos z}{z} \end{aligned} \tag{22}$$

This recurrence is unstable[2] for large values of $l$. It should hold up to $l = 20$. In spite of this, we will take $l_{max} = 13$.

Finally, the sum of the partial cross sections to get the total cross section. We will graph it as a function of the energy. The range considered will be $0.1meV \leq E \leq 3.5meV$. We can't go too close to $E = 0$ since the wave length from the equation above will get too large.

# 4 Results

First, some overall default values where chosen for the parameters, which will be later modified to see the effect they have on the result. These are:

$$l_{max} = 9, \quad \epsilon = 5.9meV, \quad \varsigma = 3.57\text{Å} \quad and \quad mesh = 2000 \tag{23}$$

where $mesh$ is the number of grid points for the radial grid.

For these values, we got the total cross section, seen in Figure 2, and the phase shifts for each $l$, seen in Figure 3, both as a function of energy.

Then, different values of $l_{max}$ were taken. Since we are expected to get good results when $l_{max}$ is 6[2] and the recurrence relation for the spherical Bessel functions becomes unstable at large $l$, we took three different values:

$$l_{max} = 4, 6, 13. \tag{24}$$

For $l_{max} = 4$, results are shown in Figures 4 and 5, while for $l_{max} = 6$ and $l_{max} = 13$ they are shown in Figures 6, 7 and 8, 9, respectively.

We see that for $l_{max} = 4$ the total cross section is not quite similar to the others. It is for $l_{max} \geq 6$ that the curves start to look alike, in shape. For low energies, all 4 curves look the same, and increasing the value of $l_{max}$ gives better results for higher energies. The difference between the total cross section for $l_{max} = 9$ and $l_{max} = 13$ is not noticeable. This is why $l_{max} = 9$ was chosen as a default value.

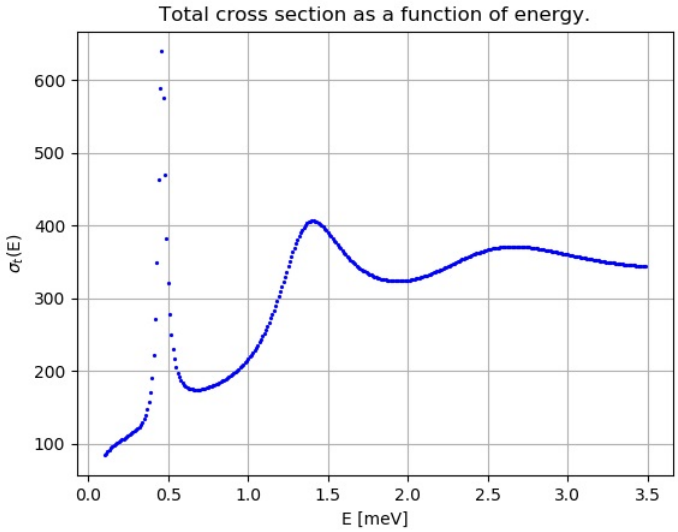


Figure 2: Total cross section as a function of energy. Default values (Eq (23)).

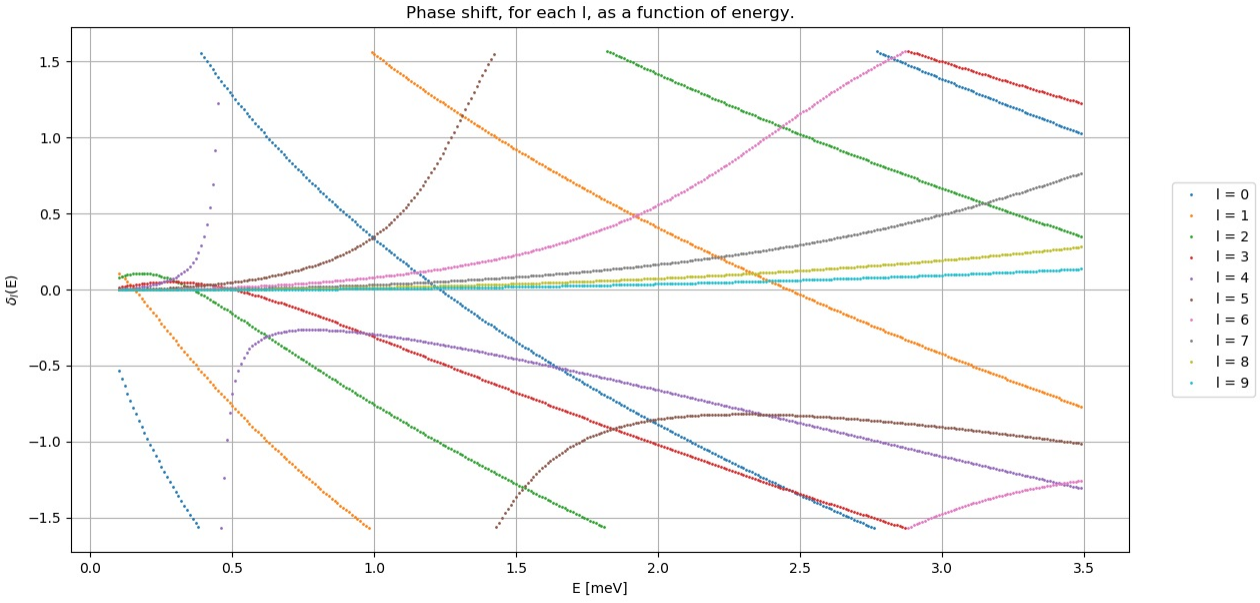


Figure 3: Phase shifts as a function of energy. Default values (Eq (23)).

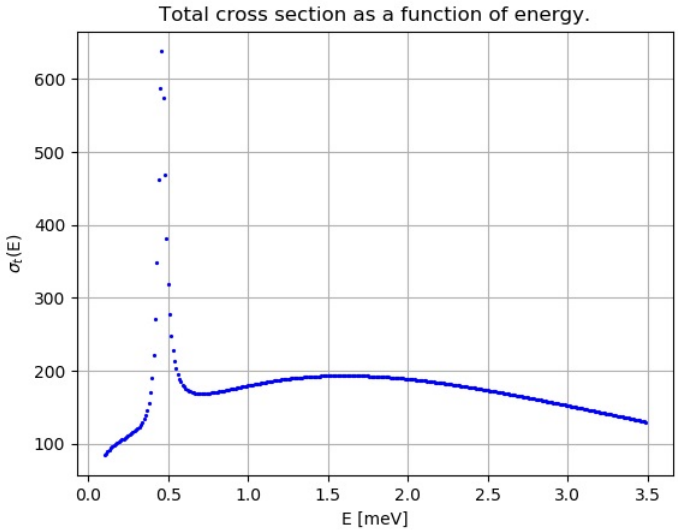


Figure 4: Total cross section as a function of energy for $l_{max} = 4$.

Another thing to notice is that, as expected, changing the value of $l_{max}$ does not affect the values of the phase shifts. For example, in Figures 5 and 7 we can see that they are the same, except that Figure 7 has also the corresponding $\delta_l$ for $l = 5, 6$.

Then, a few different values for the number of grid points in the radial grid where chosen. These were:

$$mesh = 100, 500, 1000, 3000 \tag{25}$$

Results for these values are shown in Figures 10 and 11.

One can notice that changing the number of grid points taken for the radial grid doesn't affect the overall shape of the curves. However it can be seen that a smaller value for it tends to overestimate the total cross section. The default value of $mesh = 2000$ was taken because around that value the curve pretty much stop changing when it was increased.

Then, the parameters of the Lennard-Jones potential were changed. First:

$$\epsilon = 4, 7.5 \tag{26}$$

This corresponds to rising and lowering, respectively, the minimum of the potential, without changing where it occurs. Results are shown in Figure 12.

We can see that the overall effect of changing $\epsilon$ is noticeable. The peaks in the curve shift to the left or to the right and are higher or lower whether $\epsilon$ was decreased or increased, respectively. Based on the other results, it seems that to get a better curve for these values, different values of $l_{max}$ and $mesh$ would be needed.

The value of $\varsigma$ was also modified:

$$\varsigma = 2.5, 4.5 \tag{27}$$

This corresponds to changing where the minimum for the potential occurs. Results are shown in Figure 13.

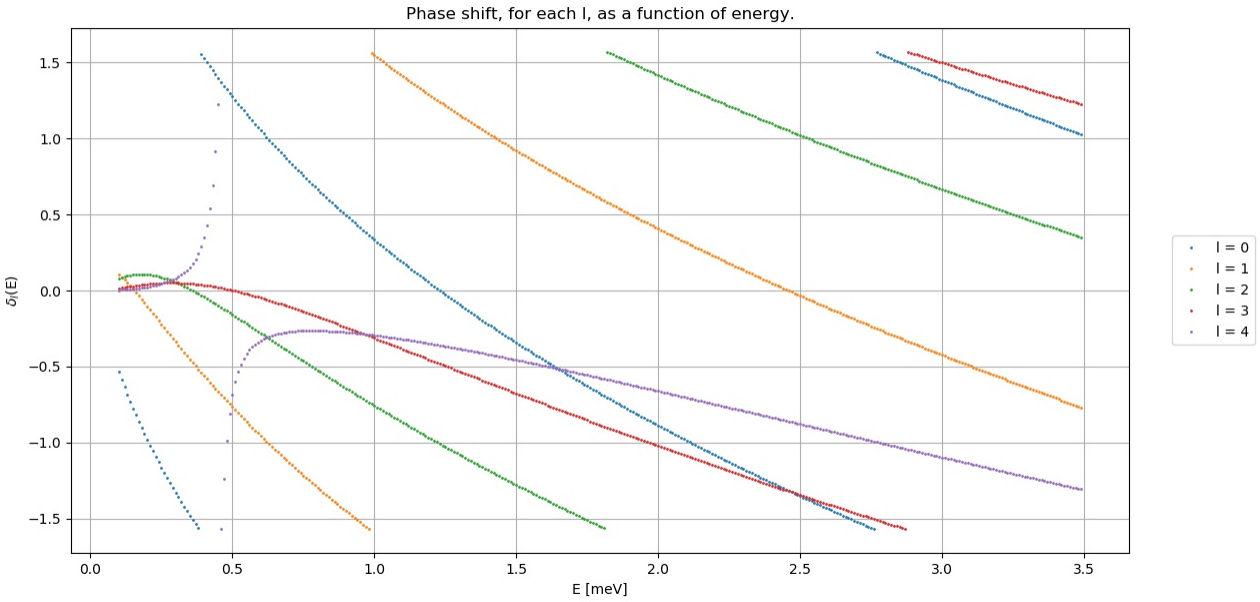


Figure 5: Phase shifts as a function of energy for $l_{max} = 4$.

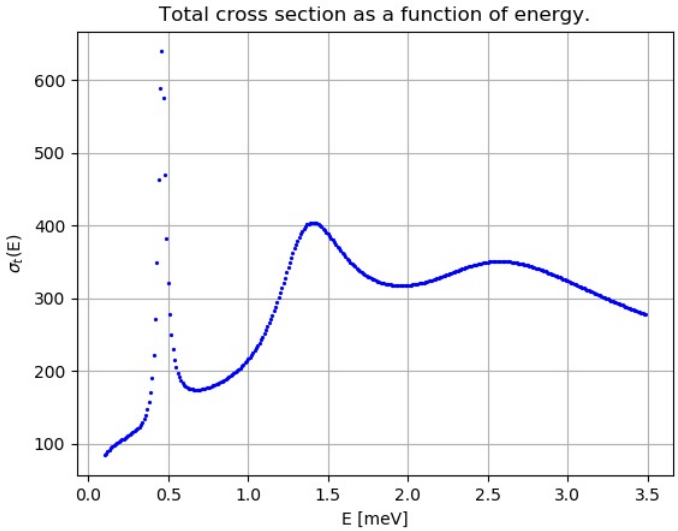


Figure 6: Total cross section as a function of energy for $l_{max} = 6$.

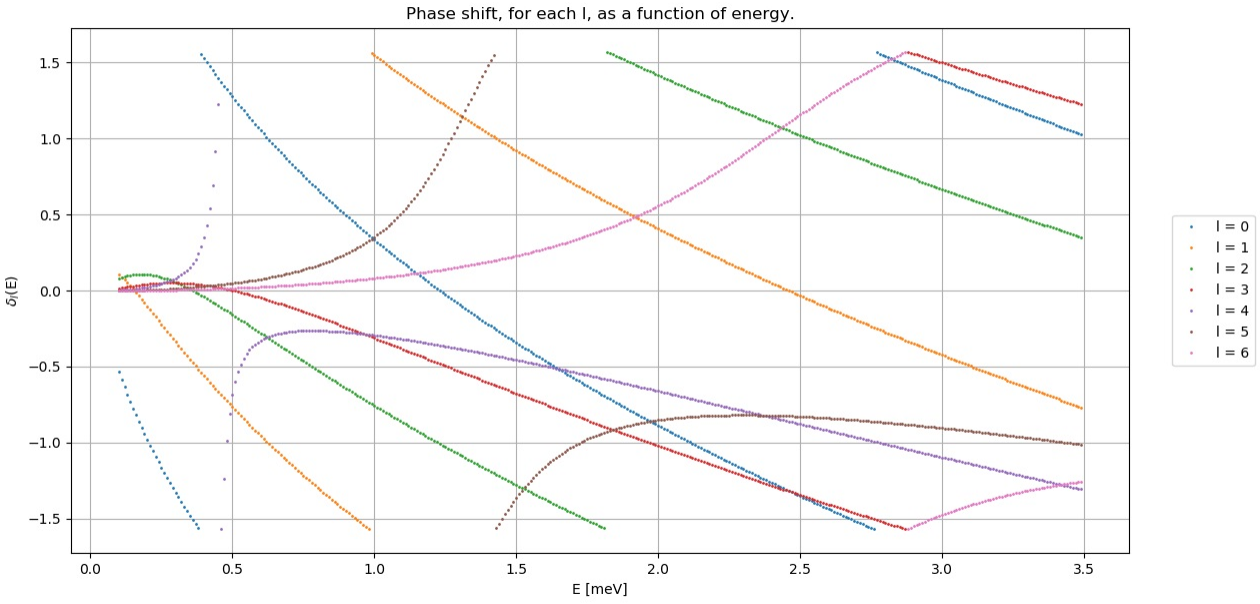


Figure 7: Phase shifts as a function of energy for $l_{max} = 6$.

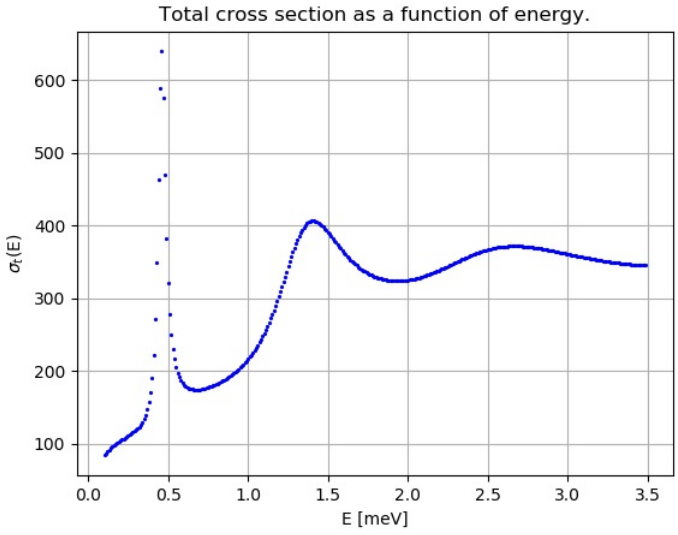


Figure 8: Total cross section as a function of energy for $l_{max} = 13$.

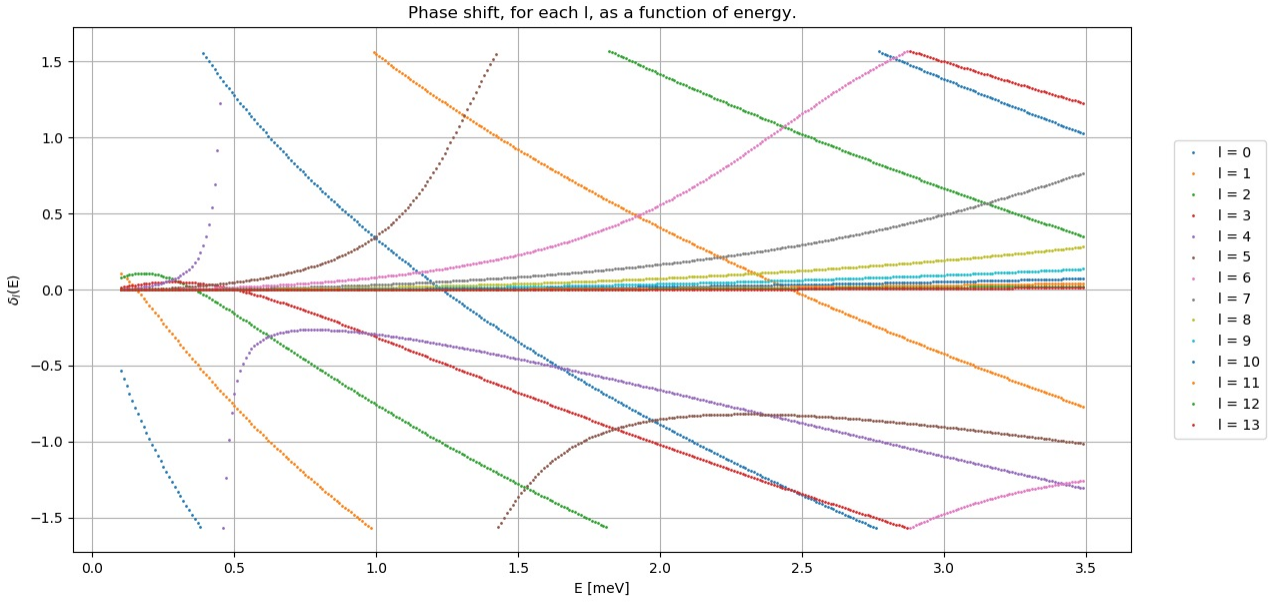


Figure 9: Phase shifts as a function of energy for $l_{max} = 13$.

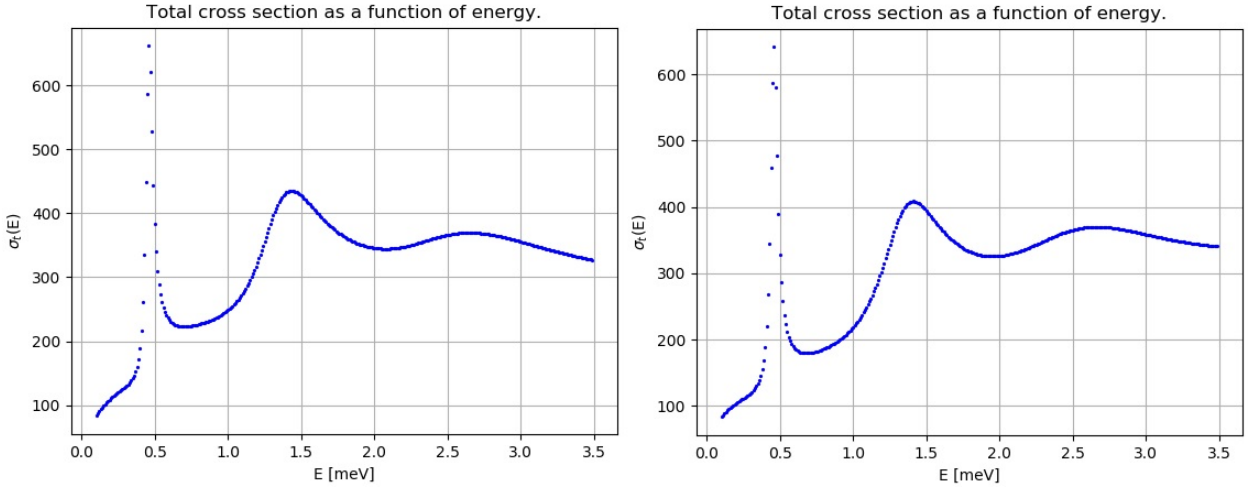


Figure 10: Total cross section as a function of energy for $mesh = 100$ (Left) and $mesh = 500$ (Right).

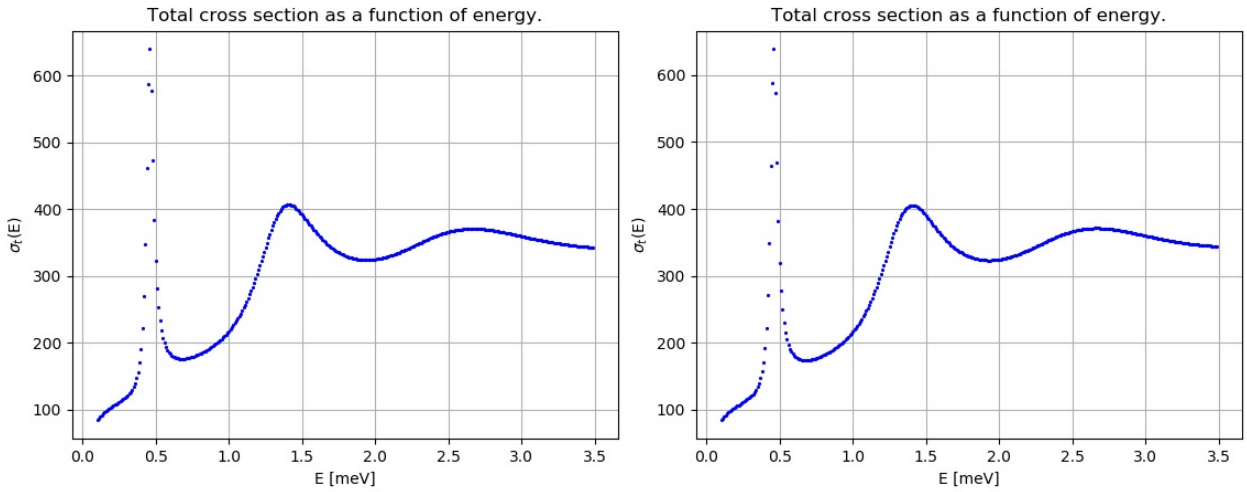


Figure 11: Total cross section as a function of energy for $mesh = 1000$ (Left) and $mesh = 3000$ (Right).

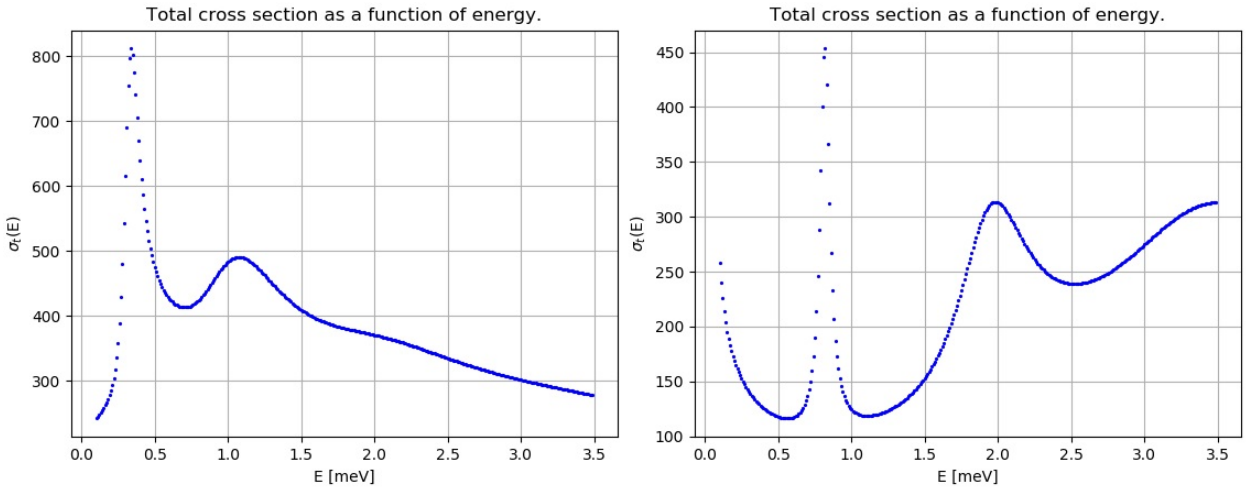


Figure 12: Total cross section as a function of energy for $\epsilon = 4$ (Left) and $\epsilon = 7.5$ (Right).

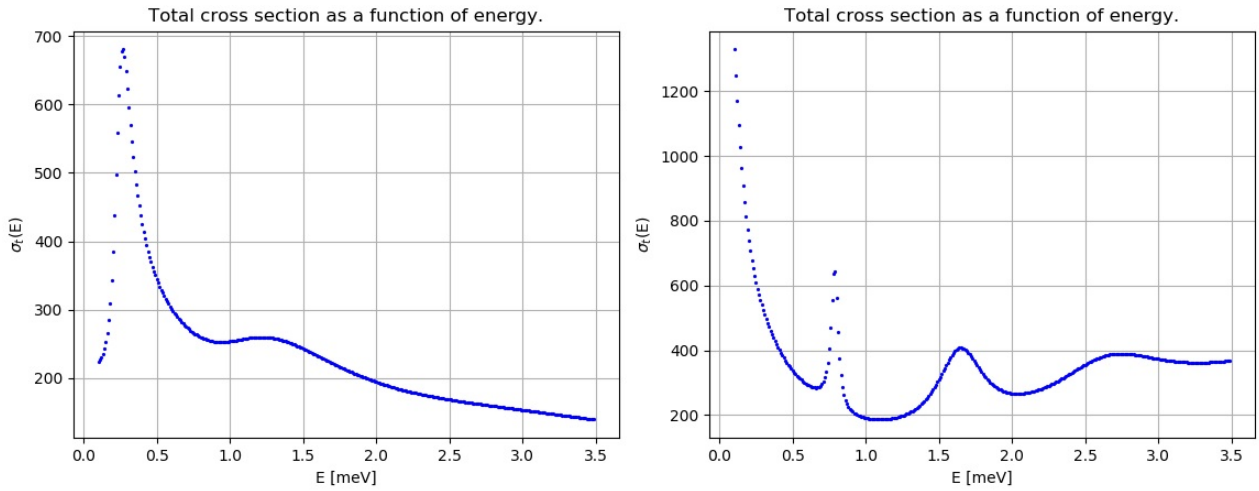


Figure 13: Total cross section as a function of energy for $\varsigma = 2.5$ (Left) and $\varsigma = 4.5$ (Right).

The overall result is similar to that of changing $\epsilon$.

It can be noted that changing $\epsilon$ and $\varsigma$ causes the cross section to diverge at lower energies, specifically when they were increased. This could be because in the implementation of the algorithm we chose some parameters based on what $\epsilon$ and $\varsigma$ were.

One last thing to mention is that, as seen in Figure 2, the cross section as three distinct spikes. This is because, it can be shown[3], that the partial cross section for a given $l$ can be written as:

$$\sigma_l(E) = \frac{4\pi}{k^2}(2l+1)\sin^2\delta_l = \frac{4\pi}{k^2}(2l+1)\frac{\Gamma^2}{4(E-E_0)^2+\Gamma^2} \tag{28}$$

where $E_0$ is the resonant energy and $\Gamma$ is the width of the resonance. Both depend on $l$ and how the logarithmic derivative, with respect to $r$, of $\chi_l$ changes as a function of energy.

We can see that when $E$ gets close to $E_0$, for a given $l$, $\sigma_l$ will be large compared to the others, and so $\sigma_t$ will present a peak there.

This happens in our case for three particular values of $l$, which are $l = 4, 5, 6$. This is why Figure 4 has only one peak. This can be seen if we plot the partial cross sections, along with the total cross section. This can be seen for values in (23) in Figure 14 while in Figure 15 the effective potential can be seen, as written in (8).

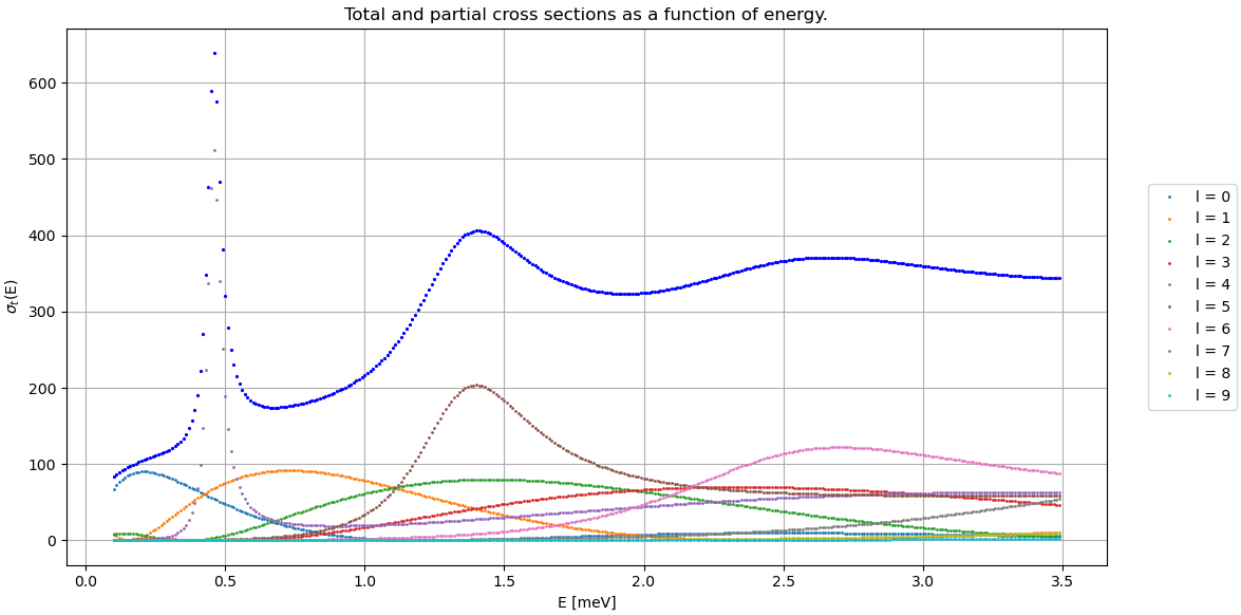


Figure 14: Total and partial cross sections for default values (Eq (23)).

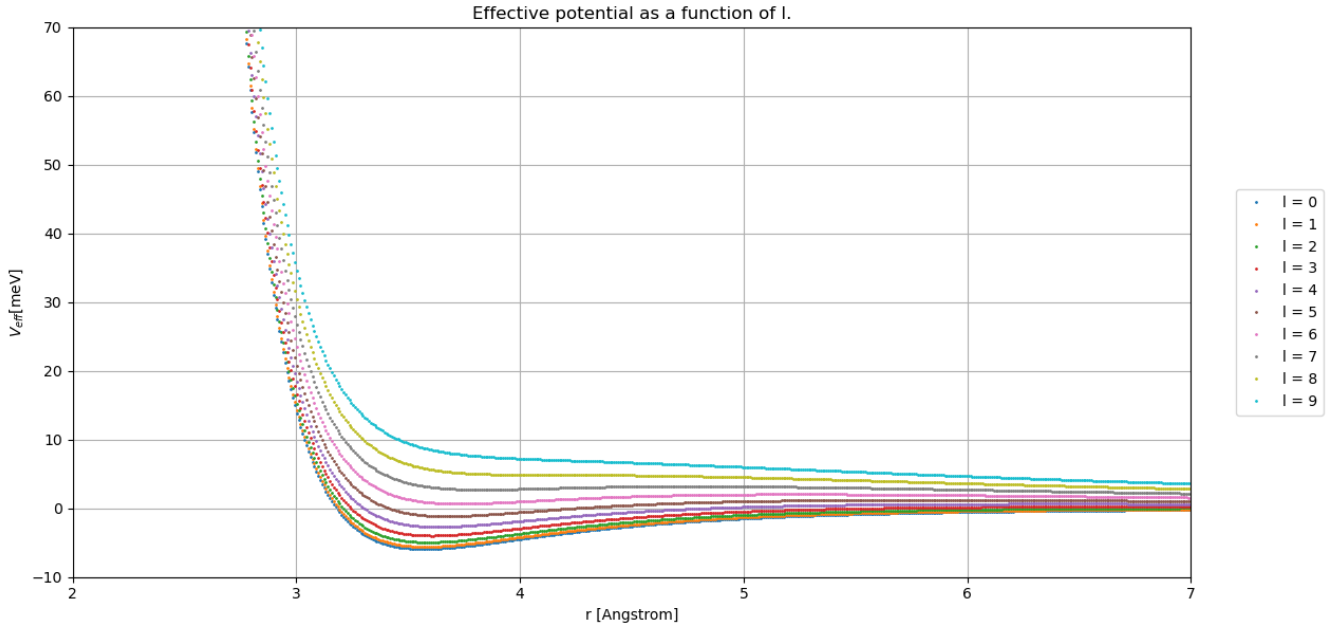


Figure 15: Effective potential as a function of $l$.

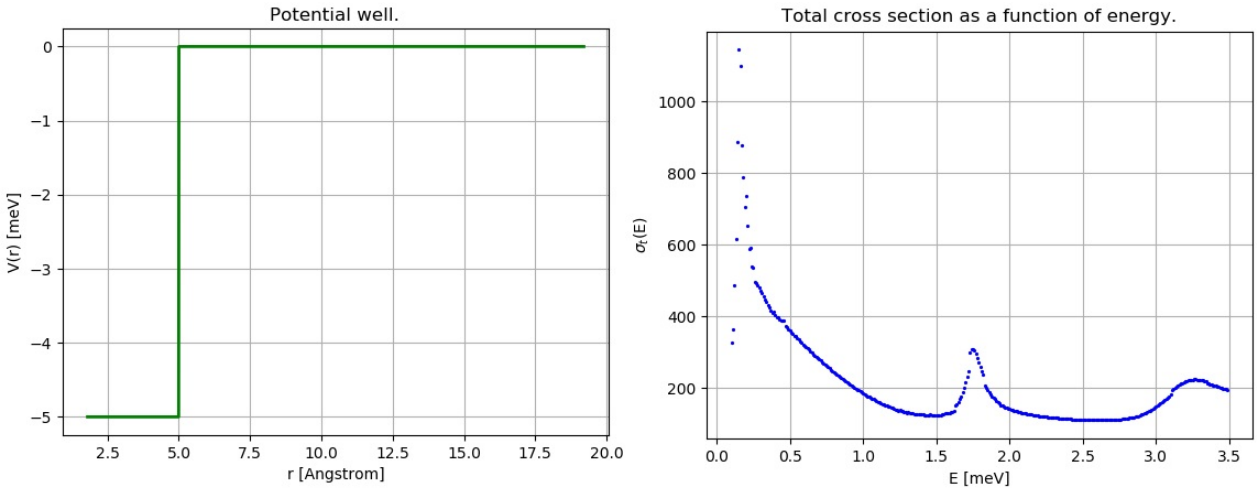


Figure 16: Potential well (left). Total cross section as a function of energy for the potential well (right).

# 5 Potential well

Now, let's consider a different potential. In particular, a potential well, seen in Figure 16, given by:

$$V(r) = \begin{cases} -5 & \text{if } r < 5 \\ 0 & \text{if } r \geq 5 \end{cases} \tag{29}$$

To implement this, we need to change both the function that sets the array for the potential and the function that sets up the initial conditions. As before, we consider that, from equation (8), we have:

$$\frac{\hbar^2}{2\mu}\frac{d^2\chi(r)}{dr^2} - \frac{\hbar^2}{2\mu}\frac{l(l+1)}{r^2}\chi(r) \sim 0 \quad for \quad r \to 0 \tag{30}$$

Then, we get:

$$r^2\frac{d^2\chi(r)}{dr^2} = l(l+1)\chi(r) \tag{31}$$

Proposing $r^\alpha$ as a solution we get:

$$\alpha(\alpha-1) = l(l+1) \quad therefore \quad \alpha_1 = l+1, \quad \alpha_2 = -l \tag{32}$$

Then, keeping the physical solution, we get, for our initial condition:

$$\chi(r) \sim r^{l+1} \quad for \quad r \to 0 \tag{33}$$

Results for this potential can be seen in Figure 16.

It can be seen that the overall result looks very similar to that of the Lennard-Jones potential. The three peaks can still be seen, and they look more spread over the grid.

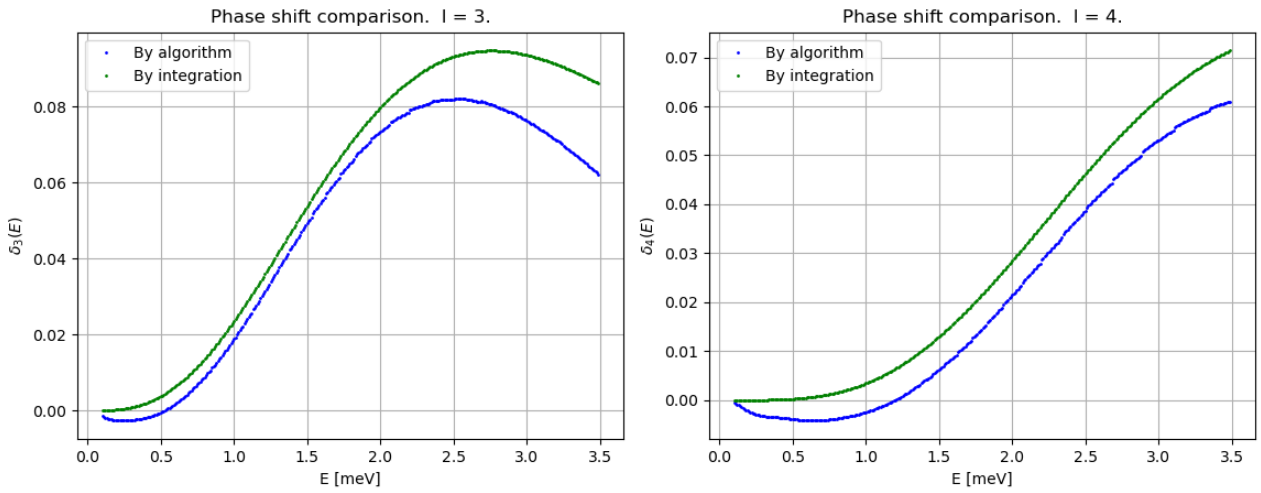


Figure 17: Phase shifts. Comparison with Born approximation for $V_0 = 0.1$.

In the limit of a weak potential, the phase shifts $\delta_l$ can be approximated[2] by the following integral:

$$\delta_l(E) \approx -\frac{2\mu}{\hbar} k \int_0^\infty r^2 j_l^2(kr) V(r) dr \quad where \quad k^2 = \frac{2\mu E}{\hbar^2} \tag{34}$$

So, we did some tests for three different wells of the form

$$V(r) = \begin{cases} -V_0 & \text{if } r < 5 \\ 0 & \text{if } r \geq 5 \end{cases} \quad with \quad V_0 = 0.1, 0.05, 0.01 \tag{35}$$

and we took $l$ from 0 to 6.

Those values for $V_0$ were hit or miss unfortunately. Some combinations gave decent results while other combinations gave not so good results. As an example, and to avoid clutter, we show results obtained for $V_0 = 0.1$ and $l = 0, 1, 3, 4$ in Figures 17 and 18. Other graphs obtained where similar. The ones shown in Figure 17 were the only ones of their kind. The others were similar to the ones shown in Figure 18.

One thing we noticed is that the phase shifts obtained by integration were never negative. This means, as we can see in Figure 18 that the values obtained via the approximation will never match with those obtained with the algorithm.

One might think that discrepancies arise from the fact that we aren't working over the whole grid, since $r$ is never zero, but even when tweaking the script to take this fact into account results were not different from the ones shown in Figures 17 and 18.

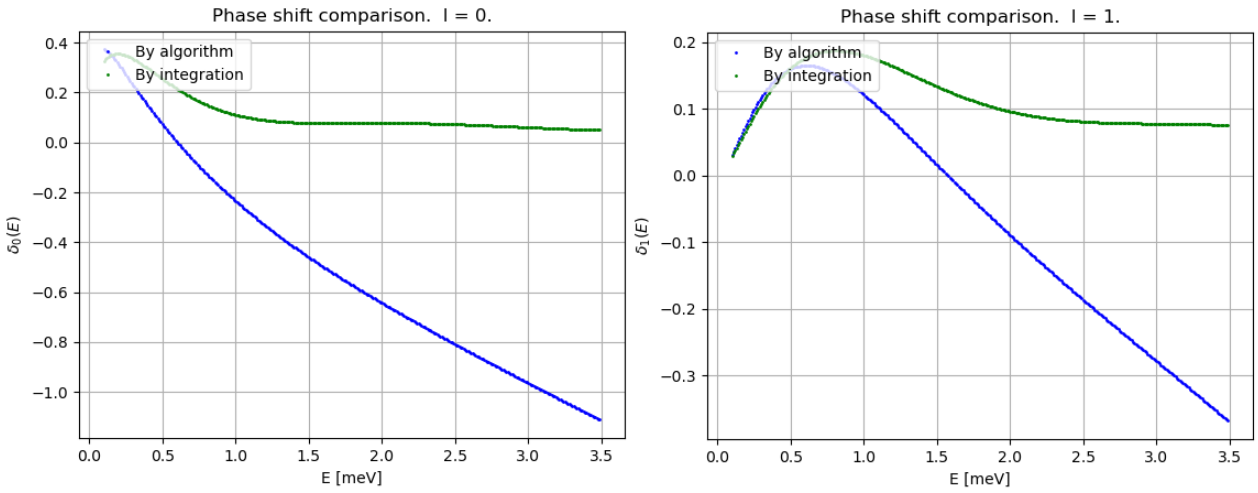


Figure 18: Phase shifts. Comparison with Born approximation for $V_0 = 0.1$.

# References


[1] Zettili, N. (2009) "*Quantum Mechanics: Concepts and Applications*". United Kingdom: John Wiley & Sons, Ltd.

[2] Giannozzi, P. (2019) "*Numerical Methods in Quantum Mechanics*". Lecture notes. University of Udine, Italy. Academic year 2018/2019.

[3] Merzbacher, E. (1998) "*Quantum Mechanics*". United States of America: John Wiley & Sons, Ltd.